Journal of Magnetic Resonance 210 (2011) 7–15

Contents lists available at ScienceDirect

Journal of Magnetic Resonance

journal homepage: www.elsevier.com/locate/jmr

Noise figure characterization of preamplifiers at NMR frequencies

J.A. Nordmeyer-Massner, N. De Zanche, K.P. Pruessmann *

Institute for Biomedical Engineering, ETH Zurich and University of Zurich, Zurich, Switzerland

ARTICLE INFO

Article history:
Received 16 December 2010
Revised 22 January 2011
Available online 3 February 2011

Keywords:
Radio frequency
Noise figure
Noise figure measurement
Noise parameters
Signal-to-noise ratio
MRI

ABSTRACT

A method for characterizing the noise figure of preamplifiers at NMR frequencies is presented. The noise figure of preamplifiers as used for NMR and MRI detection varies with source impedance and with the operating frequency. Therefore, to characterize a preamplifier's noise behavior, it is necessary to perform noise measurements at the targeted frequency while varying the source impedance with high accuracy. At high radiofrequencies, such impedance variation is typically achieved with transmission-line tuners, which however are not available for the relatively low range of typical NMR frequencies. To solve this issue, this work describes an alternative approach that relies on lumped-element circuits for impedance manipulation. It is shown that, using a fixed-impedance noise source and suitable ENR correction, this approach permits noise figure characterization for NMR and MRI purposes. The method is demonstrated for two preamplifiers, a generic BF998 MOSFET module and an MRI-dedicated, integrated preamplifier, which were both studied at 128 MHz, i.e., at the Larmor frequency of protons at 3 Tesla. Variations in noise figure of 0.01 dB or less over repeated measurements reflect high precision even for small noise figures in the order of 0.4 dB. For validation, large sets of measured noise figure values are shown to be consistent with the general noise-parameter model of linear two-ports. Finally, the measured noise characteristics of the superior preamplifier are illustrated by SNR measurements in MRI data.

1. Introduction

NMR and MRI are limited by the relative weakness of nuclear magnetism, which results in modest overall sensitivity and signal-to-noise ratio (SNR). Consequently, MR instrumentation and methods generally aim to maximize the primary signal yield of a given experiment as well as to minimize signal degradation by the detector hardware and along the remainder of the receiver chain.

With common Faraday detection the receiver chain typically consists of a coil to detect the induced electromotive force, tuning and matching circuitry, a preamplifier, and a cascade of further amplifiers to boost the signal to a level suitable for analog demodulation or direct digitization. Inevitably, each of these components adds a certain amount of noise and thus reduces the SNR below its ideal, intrinsic value [1]. The dominant noise sources are those that affect the signal when it is weakest, i.e., before it is initially amplified by typically 20 dB or more. Therefore, the most critical contributions of detector noise arise from passive components such as the coil conductor, associated circuitry and cable (if present), and the preamplifier itself (active). The magnitude of noise added by the passive components increases both with their ohmic losses and with their temperature. Therefore, in addition to using good room-temperature conductors and high-quality lumped reactances, these noise contributions can also be reduced by cryogenic cooling [2–6] and by the use of superconductors [7–11].

The noise added by the preamplifier is usually characterized by its noise figure (NF), which expresses the relative SNR degradation caused by a signal transfer or amplification stage [12]. The noise figure depends not only on the device used and the frequency of operation but also on the source impedance, i.e., the impedance that the coil presents to the preamplifier. For a given linear device and operating frequency, the noise figure is minimal at a unique optimal source impedance Z_{opt} [13,14]. Noise matching consists of transforming the complex coil impedance to yield Z_{opt}, thus ensuring optimal SNR performance of the preamplifier. Noise matching is straightforward for single-channel receivers with a fixed load. However, it is challenging and often subject to compromise for arrays of variably-loaded and mutually-coupled receiver coils [15–18], particularly when the radiofrequency (RF) wavelength is smaller than the imaging target [19,20], for large coil numbers [21–24] and with geometrically adjustable coil configurations [25–27]. In all of these situations, preamplifier noise is a key determinant of net sensitivity and must be carefully controlled.

Effective noise matching requires very accurate measurement of noise figures and their dependence on source impedance, for which a variety of established approaches exist. All these methods

* Corresponding author. Address: Institute for Biomedical Engineering, ETH Zurich and University of Zurich, Gloriastrasse 35, CH-8092 Zurich, Switzerland. Fax: +41 44 632 11 93.
E-mail address: pruessmann@biomed.ee.ethz.ch (K.P. Pruessmann).

1090-7807/$ - see front matter © 2011 Elsevier Inc. All rights reserved.
doi:10.1016/j.jmr.2011.01.025

rely on measurements of noise power at the output of the device under test (DUT). Direct measurements require power detection with absolute-level accuracy, which is challenging for low noise powers but useful for assessing large noise figures [28]. The so-called signal generator twice-power method is also most suitable for high-noise-figure devices and requires knowledge of the noise bandwidth of the instrument used for the power measurement [28]. A more common and more sensitive alternative is the Y-factor method, which is based on measuring output noise powers for different noise levels at the input of the DUT [28]. In its traditional implementation, the input noise is generated by a resistor whose temperature is varied, e.g., between room-temperature and that of liquid nitrogen [29]. However, in this approach the temperature change is much smaller than that available from dedicated, electronically-controlled noise sources that allow more sensitive, automated noise figure measurements to be made [30].

In its traditional form, the Y-factor method permits noise figure measurements only for one single source impedance, which is determined by the noise source used and is typically 50 Ω for standard telecommunications applications. It is therefore not suitable for studying the variation of the noise figure with source impedance as necessary for NMR and MRI applications. For high operating frequencies (above 1 GHz), the effective impedance of noise sources is sometimes varied with tuners based on transmission line technology [31], which however are expensive and not readily available for NMR frequencies ranging down to several tens of MHz.

To address this shortfall, the present work describes a simple method of impedance tuning for suitably low operating frequencies. In the proposed approach, reliable variation of noise temperature and impedance is achieved by a standard diode noise source followed by lumped-element circuits [32] containing both resistive and reactive components. A calibrated set of such circuits permits sampling the noise figure across the complex impedance plane at common NMR frequencies. The proposed approach is demonstrated by noise figure measurements of RF preamplifiers at 128 MHz, comparing a specifically-designed, integrated module with a generic MOSFET. The method is validated by verifying the consistency of highly overdetermined noise figure measurements with the underlying theoretical model.

2. Methods and results

2.1. Measurement Method

The noise factor F of a DUT is defined as

$$F = \frac{SNR_{input}}{SNR_{output}} = \frac{Signal_{input}/Noise_{input}}{Signal_{output}/Noise_{output}}, \quad (1)$$

where SNR_{input} and SNR_{output} denote the SNR in terms of power at the DUT's input and output, respectively. According to this definition, the noise factor depends not only on the amount of noise that the DUT adds but also on the noise level at its input. Therefore, when using the noise factor to characterize a DUT, the noise level at its input is usually assumed to amount to thermal noise at the reference temperature $T_0 = 290^\circ K$ [12]. The corresponding noise figure is then calculated by converting to decibels:

$$NF = 10 \cdot \log F. \quad (2)$$

In the Y-factor method, the noise figure of a given DUT is determined by measuring the noise power at its output in the presence of two different but well defined noise levels at its input. The ratio of the two measured output power values, N_1 and N_2, is called the Y-factor:

$$Y = \frac{N_2}{N_1}. \quad (3)$$

In present-day implementations of the Y-factor method, the input noise is typically generated by 50-Ω noise sources based on avalanche diodes. When unbiased, such a noise source produces a noise power equivalent to that of a 50 Ω resistor at room-temperature. This situation is usually called the cold state and the temperature is referred to as T_c. With reverse bias into avalanche breakdown, the noise power increases while the presented impedance is approximately the same. The noise source therefore behaves like a 50 Ω resistor at an increased temperature T_h. The two equivalent noise temperatures define the excess noise ratio,

$$ENR = \frac{T_h - T_c}{T_0}. \quad (4)$$

Based on the Y-factor and the ENR, the observed noise factor is given by

$$F = \frac{ENR}{Y - 1}. \quad (5)$$

This value, however, is only an approximation of the DUT's noise factor because it includes some noise contribution from the power meter. According to Friis' formula [12], the total noise factor of two cascaded devices is given by

$$F_{tot} = F_1 + \frac{F_2 - 1}{G_1}, \quad (6)$$

where F_1, F_2 denote the noise factors of the individual stages and G_1 is the available gain of the first device. Therefore, the measured noise factor, F_{tot}, must be corrected for that of the second stage, requiring knowledge of the available gain of the DUT (G_1) and of the noise factor of the power meter (F_2).

The available gain of the DUT can be calculated based on S-parameter measurements of the DUT and a measurement of the source impedance, expressed through the reflection coefficient Γ_s [28,33–35]:

$$G_1 = \frac{(1 - |\Gamma_s|^2)|S_{21}|^2}{|1 - S_{11}\Gamma_s|^2\left(1 - |S_{22} + \frac{S_{12}S_{21}\Gamma_s}{1 - S_{11}\Gamma_s}|^2\right)}. \quad (7)$$

F_2 can be determined with the Y-factor method in a separate calibration step by connecting the noise source directly to the power meter. This calibration makes the assumption (verified and used in the present work) that the power meter's noise factor is the same when connecting it either to the noise source or the DUT. If this assumption does not hold, F_2 must be measured specifically for the source impedance presented by the DUT. When necessary, such a preparatory noise factor measurement could be done through a first run of the proposed method, treating the power meter as the device under test and skipping the 2nd-stage correction according to Eq. (7). Based on these additional measurements, the noise factor of the DUT can be calculated by rearranging Eq. (6),

$$F_1 = F_{tot} - \frac{F_2 - 1}{G_1}, \quad (8)$$

and its noise figure is then given by Eq. (2).

With the conventional setup described thus far (Fig. 1a), the noise figure of the DUT can be measured only at the source impedance presented by the noise source, i.e., at 50 Ω. As mentioned in the introduction, a transmission-line tuner placed between the noise source and the DUT (Fig. 1b) is not practical for NMR frequencies, but the proposed approach achieves similar functionality by introducing exchangeable lumped-element tuning circuits (Fig. 1c).

In principle, any combination of resistors, capacitors, and inductors could be used to vary the effective impedance seen by the

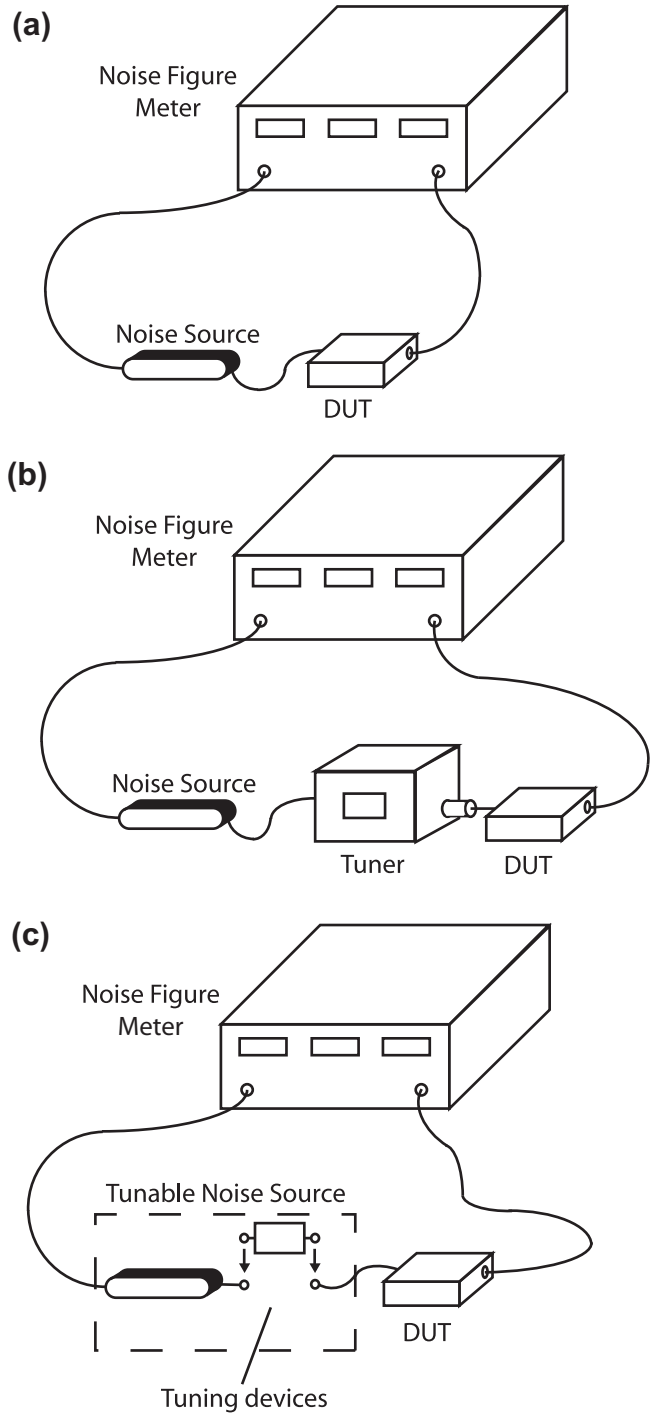

Fig. 1. Sketch of the setup for noise figure measurement. With the common setup shown in (a) only the nominal source impedance of $Z_s = 50\,\Omega$ can be presented to the DUT, irrespective of its optimal source impedance Z_{opt}. (b) For microwave measurements, this problem is frequently addressed with impedance tuners based on transmission line components which is impractical at typical NMR frequencies. In the proposed method the source impedance is tuned with exchangeable lumped-element circuits (c).

DUT. In the present implementation, one resistor per circuit, in series or parallel, was used to adjust the resistive part of the source impedance and one series inductor or capacitor was included to vary the reactive part (Fig. 2a).

The resistors act as additional sources of noise whose noise temperature remains constant when that of the diode source is switched. As a result, the net noise seen by the DUT has a different effective temperature than that of the diode source alone. For a series combination, the effective noise temperature T_{series} can be found by considering that the net noise voltage is the sum of the uncorrelated noise voltages of the two resistances. Its variance is hence given by the sum of the variances of the former,

$$\overline{U_{series}^2} = \overline{U_{diode}^2} + \overline{U_{tune}^2}, \tag{9}$$

which, according to Johnson and Nyquist [36,37] can be expanded as

$$4k_B\ \Delta f\ T_{series}(R_{diode} + R_{tune}) = 4k_B\ \Delta f\ R_{diode}T_{diode} + 4k_B\ \Delta f\ R_{tune}T_{tune} \tag{10}$$

with k_B, Δf denoting the Boltzmann constant and the considered noise bandwidth, respectively, and R_{diode}, R_{tune}, T_{diode}, T_{tune} denoting the resistances and noise temperatures of the diode source and the tuning resistor. Solving Eq. (10) for T_{series}, inserting it in Eq. (4), and considering that the temperature of the tuning resistor does not change, one obtains the effective excess noise ratio

$$ENR_{series} = \frac{R_{diode}(T_{diode,h} - T_{diode,c})}{(R_{diode} + R_{tune})T_0} = ENR_{diode}\frac{R_{diode}}{R_{diode} + R_{tune}}, \tag{11}$$

where the subscripts h and c again indicate the hot and cold states, respectively, and ENR_{diode} denotes the ENR of the diode noise source alone.

In a parallel combination, the noise currents are additive, hence

$$\overline{I_{parallel}^2} = \overline{I_{diode}^2} + \overline{I_{tune}^2} \tag{12}$$

$$4k_B\ \Delta f\ T_{parallel}\left(\frac{R_{diode}R_{tune}}{R_{diode} + R_{tune}}\right)^{-1} = 4k_B\ \Delta f\ T_{diode}R_{diode}^{-1} + 4k_B\ \Delta f\ T_{tune}R_{tune}^{-1}, \tag{13}$$

yielding

$$ENR_{parallel} = \frac{R_{tune}(T_{diode,h} - T_{diode,c})}{(R_{diode} + R_{tune})T_0} = ENR_{diode}\frac{R_{tune}}{R_{diode} + R_{tune}}. \tag{14}$$

According to Eqs. (11) and (14), in either combination the added resistor reduces the effective ENR. Therefore the choice of tuning resistors is governed by a trade-off between the attainable range of source impedances and the remaining sensitivity of the noise factor measurement. Reactances do not affect noise power and therefore the above expressions for ENR are unchanged by the presence of capacitors and inductors. The small losses that these components also exhibit in practice were neglected in the present work but could be taken into account by adding these resistances to those of the resistor.

A diode noise source of highly stable impedance (Agilent 346 A, Agilent Technologies, Santa Clara, CA, USA) was used to minimize potential systematic errors. The measured impedance varied little between the cold state $(49.7 + 0.6i)\,\Omega$ and the hot state $(49.6 + 0.7i)\,\Omega$, but this stability comes at the expense of a merely moderate ENR of 5.29 dB. Therefore, the range of resistors in the tuning circuits was chosen carefully to maintain sufficiently high ENRs for all measurements. For series combinations, $0\,\Omega$ (i.e., a short circuit), $18\,\Omega$, $39\,\Omega$, or $68\,\Omega$ were used, while parallel combinations were implemented with $33\,\Omega$, $56\,\Omega$, or $150\,\Omega$. The resulting effective ENRs, calculated according to Eqs. (11) and (14), were between the maximum of 5.29 dB and 1.28 dB, which is still sufficient for robust use of the Y-factor method. All resistor configurations were combined with different reactive components in series according to Fig. 2a, using capacitors between 5.1 pF and 220 pF and inductors between 2.7 nH and 220 nH. The tuning circuits were realized on small FR4 circuit boards and shielded against external RF interference with 70 μm copper foil. Fig. 2b shows the resulting set, comprising more than 70 different modules.

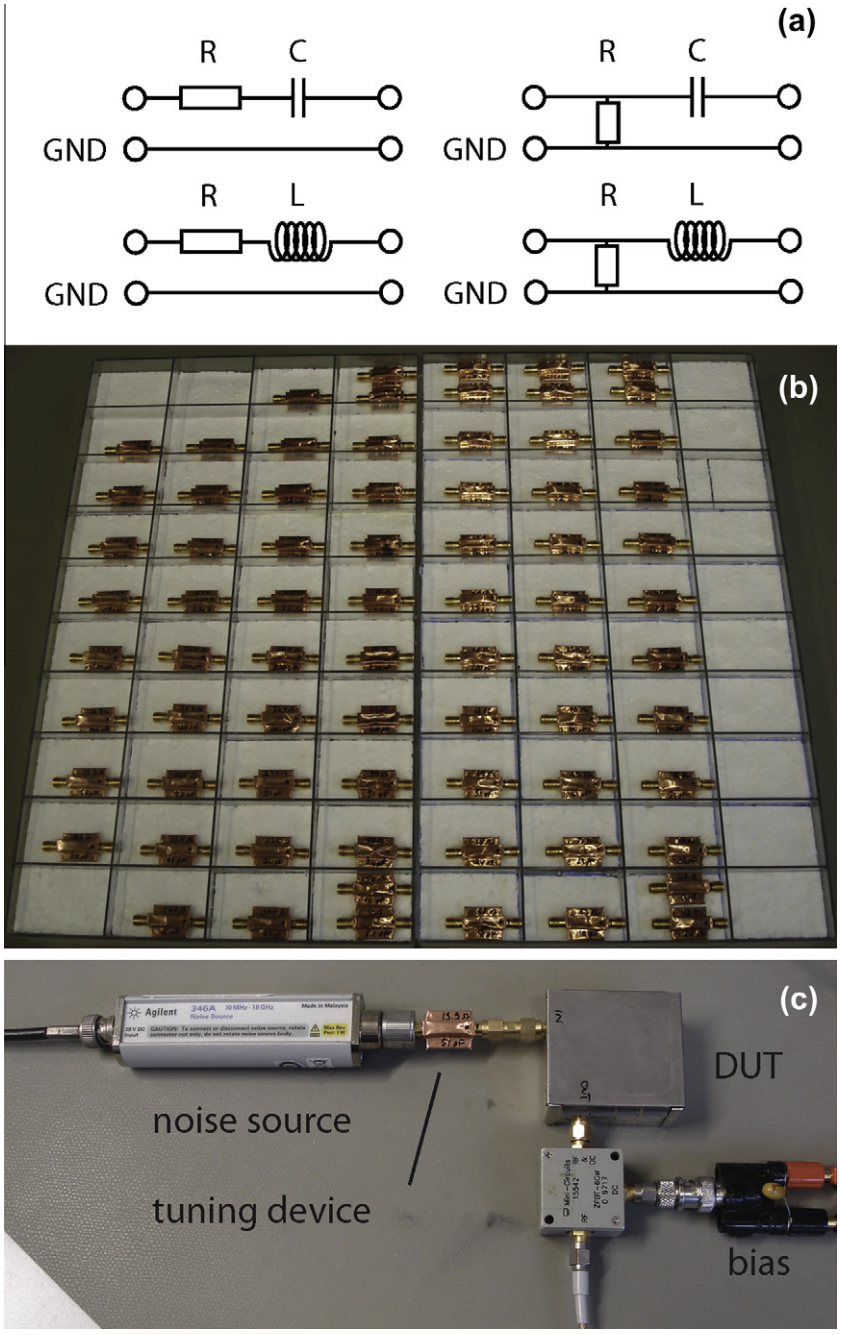

Fig. 2. (a) Four different types of tuning circuits were constructed, each combining one resistive and one reactive component. (b) Complete set of tuning circuits yielding source impedances with increasing resistive parts (left to right) and increasing reactive parts (top to bottom). (c) Measurement setup with noise source, shielded tuning circuit and a shielded box containing the DUT.

Using SMA connectors the modules are inserted individually between the noise source and a shielded box containing the DUT (Fig. 2c). The actual source impedance thus presented to the DUT was measured for each tuning circuit to capture the variability of the lumped elements as well as parasitic losses and reactances. All measurements of source impedances and S-parameters were performed with an Agilent ENA E5071C network-analyzer (Agilent Technologies, Santa Clara, CA, USA).

Noise power measurements were performed with an HP 8970A noise figure meter (from the same manufacturer). This device controls the biasing of the noise source, performs measurements of the noise powers N_1 and N_2 in the cold and hot states, respectively, and automatically translates them into resulting noise factors based on Eqs. (3) and (5). It also includes elimination of the noise contribution of the power meter (Eq. (8)). However, in the instrument's built-in procedure this step is based on the insertion gain, which is easier to determine, rather than the available gain. To remove the resulting error, noise factors obtained from the noise figure meter were corrected according to Eq. (8):

$$F_1^{corr} = F_1 + (F_2 - 1) \cdot \left(\frac{1}{G_i} - \frac{1}{G_a} \right), \tag{15}$$

where G_i, G_a denote, respectively, the DUT's insertion gain and available gain which is determined using Eq. (7). Finally, when a lumped tuning circuit was used, the resulting noise factor (Eq. (5)) was

corrected to account for the reduced effective ENR by multiplying F_1 by the ratio of the nominal and effective ENRs (Eqs. (11) and (14)).

The proposed method of noise figure characterization is demonstrated for two MR preamplifiers: an integrated preamplifier with an input matching circuit designed for operation at 128 MHz (InVivo, Gainsville, FL, USA) and a simple generic module based on an unmatched BF998 MOSFET. An initial set of experiments served to gain a rough picture of the degree of frequency dependence of these preamplifiers. For this purpose, noise figure measurements at 50 Ω, i.e., without a tuning circuit, were performed across the frequency range of 60 MHz to 300 MHz, in steps of 5 MHz. Additionally, the preamplifiers' insertion gains were measured at the same frequencies, using the noise figure meter. The results of these measurements are depicted as solid lines in the graphs plotted in Fig. 3. While the untuned MOSFET preamplifier shows only moderate frequency dependence, the noise figure and the gain of the dedicated MR preamplifier exhibit substantial spectral variation, illustrating the need to measure these quantities for each device to ensure consistency.

Subsequently, the impedance tuning approach was used to measure the noise figure of both preamplifiers at varying source impedance while keeping the frequency fixed at 128 MHz. The results of these measurements are shown in Fig. 4, in which the noise figure is plotted against the nominal values of the presented resistance and inductance or capacitance. To gauge the precision of these measurements, those of the integrated preamplifier were repeated three times on different days, resulting in variations of 0.01 dB or less.

2.2. Linear Noise Model and Noise Parameter Fit

Relying on a limited set of fixed tuning circuits, the method described above permits noise factor measurement only for a finite set of source impedances. However, such measurements can be expanded into a more complete picture if the noise factor as a function of source impedance obeys a sufficiently simple model. The noise behavior of a general linear two-port can be modeled as [13,14,38,39]

$$F = F_{min} + \frac{R_n}{G_s}|Y_s - Y_{opt}|^2 \tag{16}$$

where F_{min} denotes the minimal noise factor, $Y_s = Z_s^{-1} = G_s + iB_s$ is the source admittance, $Y_{opt} = Z_{opt}^{-1} = G_{opt} + iB_{opt}$ is the optimal source admittance at which F_{min} is realized, and R_n is the so-called noise correlation resistance, which determines the sensitivity of the noise

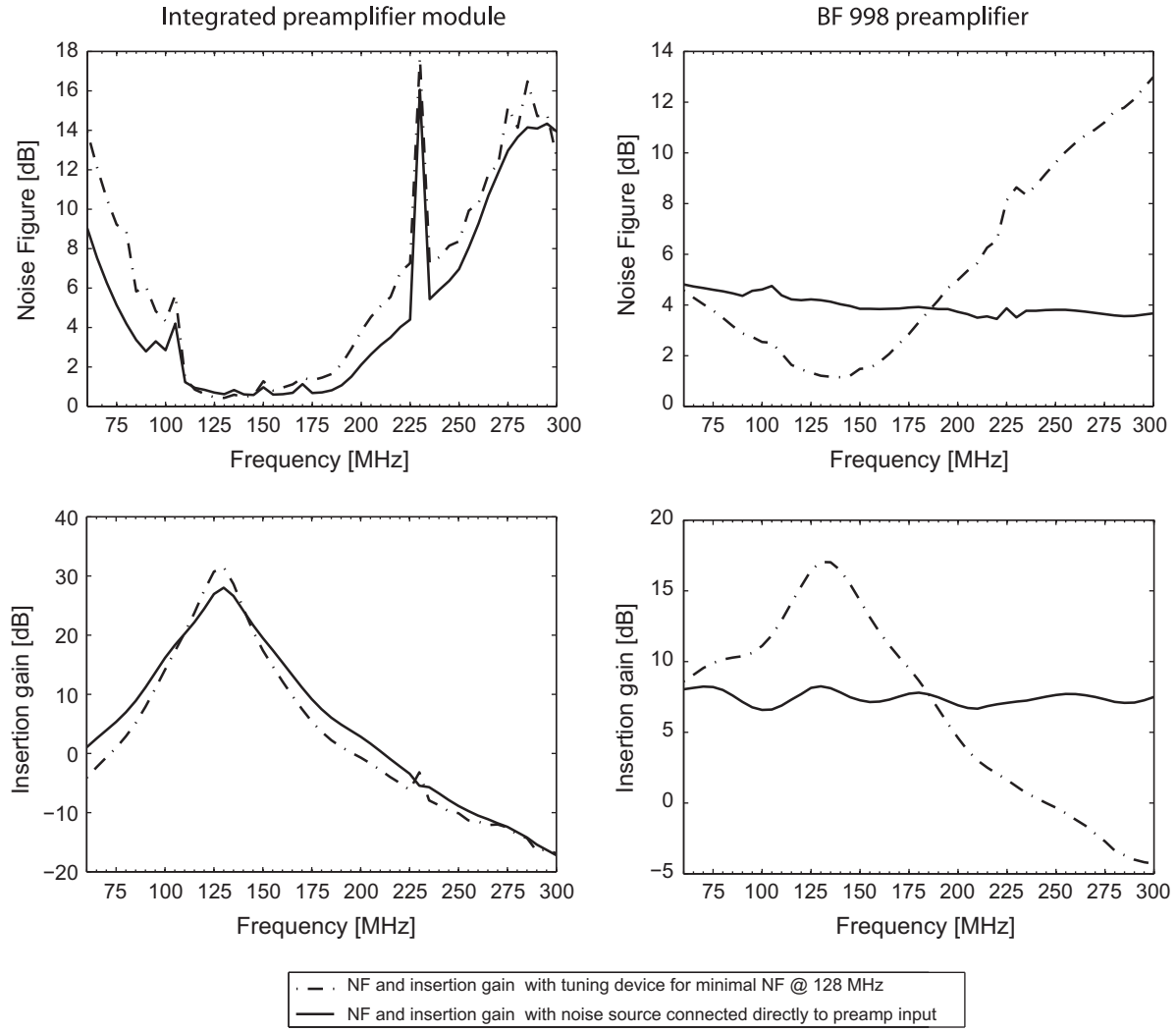

Fig. 3. Noise figure (top) and insertion gain (bottom) of the integrated preamplifier (left) and the BF998 module (right). Solid lines show measurements obtained at Z_s = 50 Ω, i.e., with the noise source connected directly. Dashed measurements were obtained at $Z_s \approx Z_{opt}$ of each preamplifier, using the closest fitting tuning circuit. Both plots show the measurements without available-gain correction. The noise figure peaks at 105 MHz and 230 MHz are likely due to environmental interference at these frequencies.

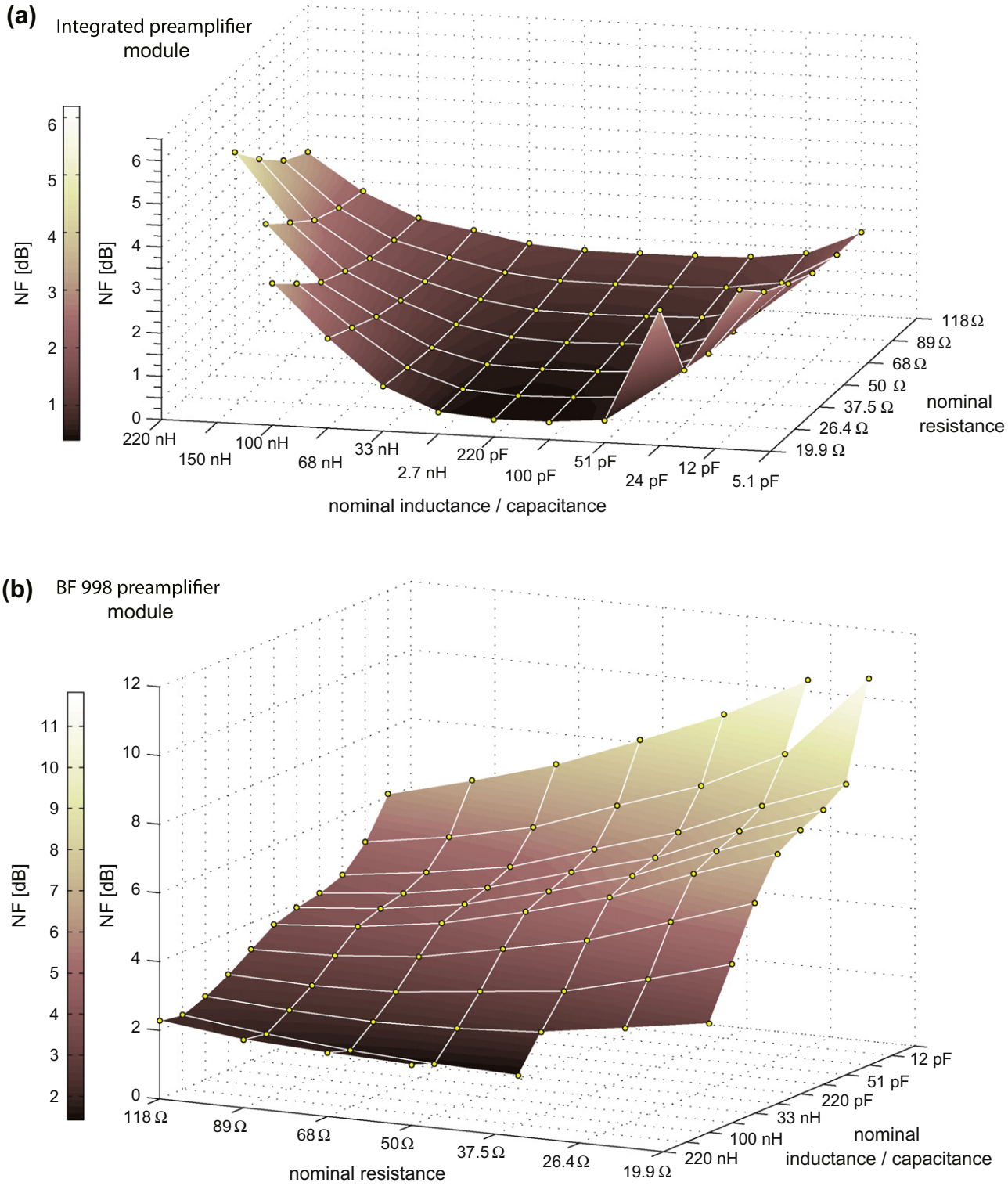

Fig. 4. Noise figures of the two preamplifiers plotted against the nominal resistances and reactive components of the circuits used for tuning the source impedance.

factor to the source admittance. Within this model, F_{min}, R_n, G_{opt}, and B_{opt} are usually referred to as the *noise parameters*.

Noise parameters can be determined by measuring the noise factor at different source impedances (or admittances, respectively) and fitting Eq. (16) to the measured values. To simplify fitting, the right-hand side of Eq. (16) can be rewritten as a linear expression in four alternative parameters a, b, c, d [38,39]:

$$F = a + bG_s + \frac{c + bB_s^2 + dB_s}{G_s}, \tag{17}$$

which relate to the original ones according to

$$F_{\min} = a + \sqrt{4bc - d^2}, \tag{18}$$

$$R_n = b, \tag{19}$$

$$G_{opt} = \frac{\sqrt{4bc - d^2}}{2b}, \tag{20}$$

$$B_{opt} = \frac{-d}{2b}. \tag{21}$$

The parameters a, b, c, d can be obtained straightforwardly by least-squares fitting, yielding the noise parameters via Eqs. (18)–(21). In principle, four noise factor measurements at different source impedances are sufficient to determine the noise parameters. A larger number of noise factor samples over-determine the noise model and improve the accuracy of the fitted noise parameters by implicit averaging of measurement noise and errors.

Table 1 shows the results of fitting the noise model to the data shown in Fig. 4. The integrated preamplifier offers substantially better noise properties, namely, a lower minimum noise figure and a much lower correlation resistance, indicating that the noise figure increases less quickly with deviations from the optimal source impedance. These properties are also evident from Fig. 5, which shows contour plots of the fitted noise figure functions along with the underlying sampling positions in the Smith chart of the source impedance. Due to the vast over-determination in this case, the consistency of the measured noise figure values with the fitted model gives a good indication of the measurement accuracy. The root-mean-square model violation was 0.11 dB for the BF998 preamplifier and 0.08 dB for the integrated module, indicating measurement errors of similar magnitude.

Based on the fitted noise models, the initial study of frequency dependence was repeated with approximate noise matching at 128 MHz. For these measurements, each preamplifier was connected to the noise source through the tuning circuit that brought the source impedance closest to the respective Z_{opt}. Again, the noise figure and the insertion gain were measured between 60 MHz and 300 MHz. The results are shown as dashed plots in Fig. 3. They illustrate that noise matching improved the noise figure of the integrated preamplifier only slightly, reflecting the small correlation resistance of this device and the fact that its optimal source impedance is relatively close to 50 Ω. Its gain improved more significantly, which improves the noise situation indirectly by reducing the SNR effects of subsequent noise contributions along the receive chain (see Eq. (8)). The noise figure peak around 230 MHz occurred with both matching conditions and is attributed to interference at this frequency. For the BF998 preamplifier, noise matching reduced the noise figure at 128 MHz significantly, reflecting the higher correlation resistance and a greater deviation of Z_{opt} from 50 Ω. With noise matching, this module's noise figure and gain exhibit distinct optima around 128 MHz.

Table 1
Noise parameters and reflection coefficients of the two preamplifiers. The noise parameters were obtained by least-squares fitting of noise figure measurements.

	BF998	Integrated preamplifier
F_{min}	1.3915	1.1011
NF_{min} (dB)	1.435	0.42
R_n (Ω)	97.64	1.35
G_{opt} (S)	0.0018	0.0373
B_{opt} (S)	−0.0036	−0.0254
R_{opt} (Ω)	110.97	18.31
X_{opt} (Ω)	224.15	12.47
RMS fit error (dB)	0.11	0.08
S11 magn. (dB)	−0.51	−2.39
S11 phase (°)	−31.63	171.37

2.3. SNR measurements

To illustrate the measured noise characteristics and the necessity of noise matching, the SNR yield of MRI was studied using the integrated preamplifier in varying matching conditions. A cuboid container ($20 \times 25 \times 8$ cm^3) filled with a phantom solution (NaCl 2000 mg/L, $CuSO_{4.5}(H_2O)$ 770 mg/L) was imaged in a 3T whole-body MRI system (Philips Achieva, Philips Healthcare, Best, The Netherlands), using a rectangular single-loop receiver coil (5×10 cm^2). The coil was connected to the integrated preamplifier through a π matching network [18,26] containing a variable parallel capacitor for matching adjustment. The preamplifier output was connected to the regular receive chain of the MRI system.

The preamplifier was initially noise-matched according to its measured Z_{opt} and its matching was then varied in four steps by adjusting the variable capacitor. All matching adjustments were made in the magnet bore and monitored by network-analyzer measurements of the resulting source impedances. For each matching setting, the resulting noise variance of the receiver channel was assessed by data acquisition without NMR excitation and imaging was performed in a transverse slice with a standard gradient-echo sequence. Maps of the resulting image SNR were calculated using the method described in Ref. [27] and mean SNR values were obtained by averaging over a fixed region close to the receiver coil (Fig. 6). The resulting SNR values (in terms of power) are shown in Table 2, reflecting progressive SNR loss with deviation from optimal matching. For comparison, the corresponding preamplifier noise figures were calculated from the measured noise parameters and source impedances. The last column of Table 2 shows the resulting noise figure degradation. These numbers and the corresponding plots in Fig. 7 confirm that the observed SNR loss was caused predominantly by noise mismatching of the preamplifier. Additional SNR losses of up to 0.2 dB are attributed to small changes in the gains of both the preamplifier and the matching network, which occur along with the matching changes.

3. Discussion

The proposed method has been shown to permit measuring the noise figure of preamplifiers at common NMR frequencies and for variable source impedance. This is achieved by impedance tuning with lumped elements rather than transmission-line tuners which would be prohibitively large for NMR frequencies. Comparison with the theory of linear noisy two-ports indicates a measurement accuracy of about 0.1 dB, corresponding to SNR uncertainty of 1% and just over 2% in amplitude and power terms, respectively. Noise factor measurements at over 70 different source impedances yielded strong over-determination of the two-port noise model, likely yielding even higher accuracy of fitted noise parameters.

The proposed method involves a number of calibration and correction steps, which allow it to be robust and accurate. Specifically, ENR correction for the tuning circuits, measurement of effective source impedances, and available-gain correction need to be performed. Tight shielding of the entire setup against environmental RF perturbations has proven essential particularly for measuring small noise figures. Finally, impedance stability of the noise source and careful calibration, setup and warm-up of the measurement instruments have equally been found to be vital.

In the current implementation, the tuning circuits include lumped resistances as well as reactances to adjust the net source impedance. Alternatively, they could also be constructed from reactive components alone. This approach would have the benefit of overall larger effective ENRs and could thus render the Y-factor method more sensitive if necessary. Notwithstanding, ENR correction would likely still be necessary due to parasitics and the losses

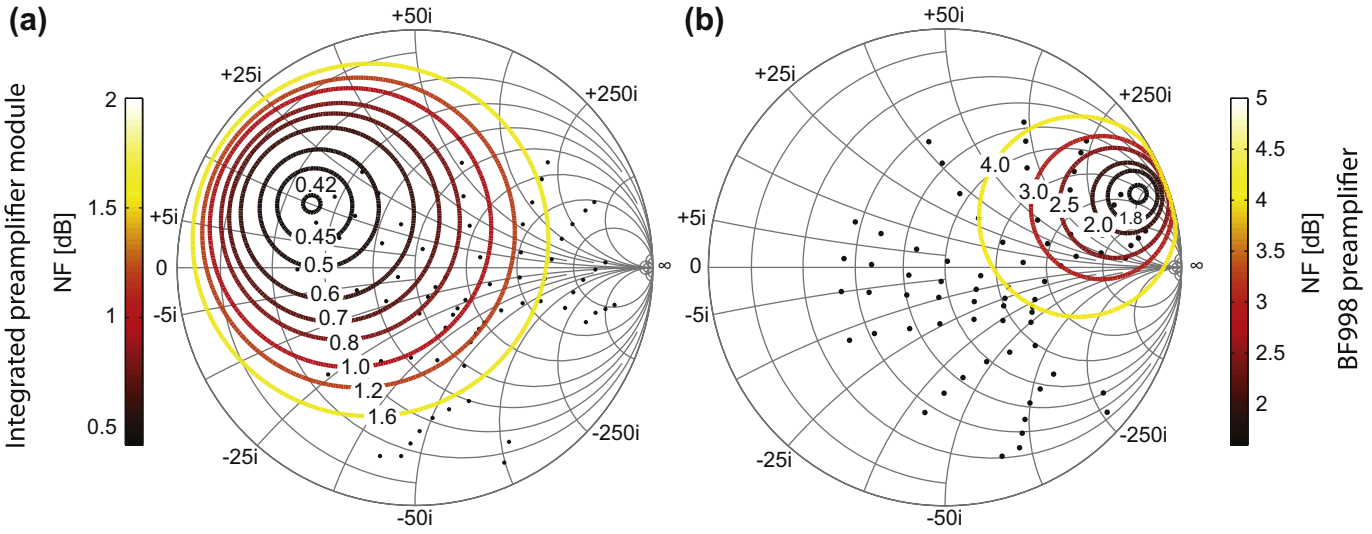

Fig. 5. Measured noise figures of the integrated preamplifier (a) and the BF998 module (b), plotted on the Smith chart of the source impedance. The smallest NF circles represent 0.42 dB and 1.6 dB, respectively. Dots indicate points of noise figure measurement. Circles of constant noise figure were calculated from fitted noise parameters.

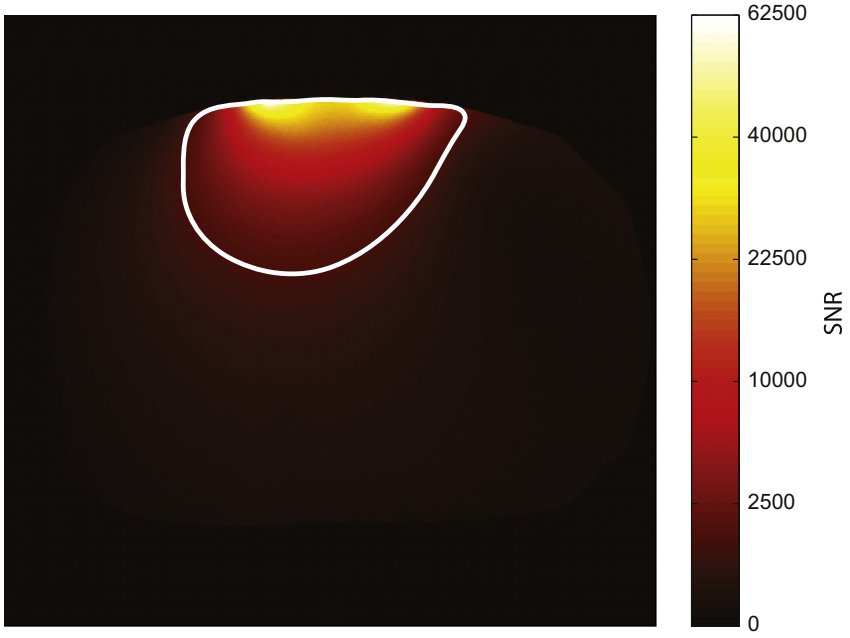

Fig. 6. SNR map of MRI data obtained with a surface receiver coil and the integrated preamplifier module. SNR maps were collected for the noise-matched situation (shown) and increasing noise mismatch (not shown). For each matching, an overall SNR figure was calculated by averaging over the shown region of interest.

Table 2
Image SNR obtained with the integrated preamplifier using noise matching (first row) and increasing noise mismatch. SNR values in the second column are given in power terms according to the notation underlying Eq. (1).

Source impedance (Ω)	SNR	SNR (dB)	SNR loss (dB)	Degradation of preamplifier NF (dB)
18.4 + 7.4i	21,360	43.30	–	–
25.5 + 6.5i	21,002	43.22	0.08	0.00
38.2 + 11.1i	20,655	43.15	0.15	0.05
42.0 + 47.3i	19,005	42.79	0.51	0.37
14.3 + 52.6i	15,828	41.99	1.31	1.10

of the tuning circuits would be more challenging to determine accurately.

Accurate noise figure measurement is expected to benefit the development and assessment of NMR preamplifiers as well as the design and matching of NMR probes. Noise figure stability is especially important when variable loading, variable coil-to-coil coupling, or flexible coil geometry need to be accommodated. In probes with fixed matching, these conditions require particularly

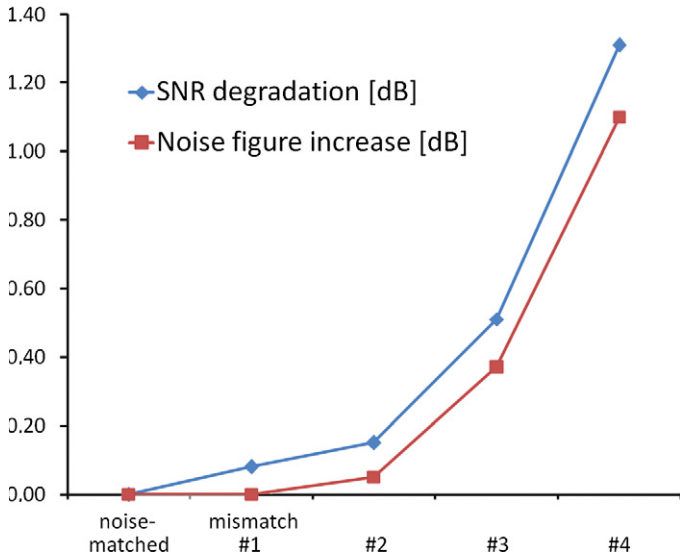

Fig. 7. Plot of the SNR loss incurred with four levels of increasing noise mismatch (Table 2) relative to the noise-matched situation. The squares indicate the underlying increase in noise figure according to the noise parameters measured on the bench. The additional SNR losses of up to 0.2 dB are caused by concomitant small changes in gain of the preamplifier and the matching network.

low sensitivity of the noise figure to changes in source impedance, i.e., a very low correlation resistance. A promising alternative, especially for coil arrays, is dynamic matching adjustment based on automated source impedance measurements [40,41]. This approach opens up the possibility to perform noise matching based on the actual impedance matrix that a receiver array presents in a given experimental situation. It thus highlights the important distinction between noise matching of a single coils and noise matching of arrays [42] and calls for reliable modeling of the noise behavior of coupled, loaded receivers. In this area of development, too, accurate noise figure characterization of the preamplifiers involved will be an essential step.

References

[1] W.A. Edelstein, G.H. Glover, C.J. Hardy, R.W. Redington, The intrinsic signal-to-noise ratio in NMR imaging, Magn. Reson. Med. 3 (1986) 604–618.
[2] P. Styles, N.F. Soffe, C.A. Scott, D.A. Crag, F. Row, D.J. White, P.C.J. White, A high-resolution NMR probe in which the coil and preamplifier are cooled with liquid helium, J. Magn. Reson. 60 (1984) 397–404.
[3] A.S. Hall, B. Barnard, P. Mcarthur, D.J. Gilderdale, I.R. Young, G.M. Bydder, Investigation of a whole-body receiver coil operating at liquid nitrogen temperatures, Magn. Reson. Med. 7 (1988) 230–235.
[4] M. Jerosch-Herold, R.K. Kirschman, Potential benefits of a cryogenically cooled NMR probe for room-temperature samples, J. Magn. Reson. 85 (1989) 141–146.
[5] A.C. Wright, H.K. Song, F.W. Wehrli, In vivo MR micro imaging with conventional radiofrequency coils cooled to 77 degrees K, Magn. Reson. Med. 43 (2000) 163–169.
[6] L. Darrasse, J.C. Ginefri, Perspectives with cryogenic RF probes in biomedical MRI, Biochimie 85 (2003) 915–937.
[7] A.S. Hall, N.M. Alford, T.W. Button, D.J. Gilderdale, K.A. Gehring, I.R. Young, Use of high temperature superconductor in a receiver coil for magnetic resonance imaging, Magn. Reson. Med. 20 (1991) 340–343.
[8] R.D. Black, T.A. Early, P.B. Roemer, O.M. Mueller, A. Mogro-Campero, L.G. Turner, G.A. Johnson, A high-temperature superconducting receiver for nuclear magnetic resonance microscopy, Science 259 (1993) 793–795.
[9] J.G. van Heteren, T.W. James, L.C. Bourne, Thin film high temperature superconducting RF coils for low field MRI, Magn. Reson. Med. 32 (1994) 396–400.
[10] J. Wosik, K. Nesteruk, L.-M. Xie, M. Strikovski, F. Miller Jr, J.H. Wang, M. Bilgen, P.A. Narayana, High-Tc superconducting RF receiver coils for magnetic resonance imaging of small animals, Physica C 341–348 (2000) 2561–2564.
[11] J.C. Ginefri, L. Darrasse, P. Crozat, High-temperature superconducting surface coil for in vivo microimaging of the human skin, Magn. Res. Med. 45 (2001) 376–382.
[12] H.T. Friis, Noise figures of radio receivers, Proc. IRE 32 (1944) 419–422.
[13] Noise in linear two-ports. IRE Standards on Electron Tubes: Definitions of Terms, 1962 (62 IRE 7. S2), Proc. IRE 51 (1963), 434.
[14] H. Fukui, Available power gain, noise figure, and noise measure of 2-ports and their graphical representations, IEEE Trans. Circuit Theory 13 (1966) 137–142.
[15] P.B. Roemer, W.A. Edelstein, C.E. Hayes, S.P. Souza, O.M. Mueller, The NMR phased array, Magn. Reson. Med. 16 (1990) 192–225.
[16] C.E. Hayes, P.B. Roemer, Noise correlations in data simultaneously acquired from multiple surface coil arrays, Magn. Reson. Med. 16 (1990) 181–191.
[17] D. Kwiat, S. Einav, G. Navon, A decoupled coil detector array for fast image acquisition in magnetic resonance imaging, Med. Phys. 18 (1991) 251–265.
[18] A. Reykowski, S.M. Wright, J.R. Porter, Design of matching networks for low noise preamplifiers, Magn. Reson. Med. 33 (1995) 848–852.
[19] G. Adriany, P.-F. van de Moortele, F. Wiesinger, S. Moeller, J.P. Strupp, P. Andersen, C. Snyder, X. Zhang, W. Chen, K.P. Pruessmann, P. Boesiger, T. Vaughan, K. Ugurbil, Transmit and receive transmission line arrays for 7 Tesla parallel imaging, Magn. Reson. Med. 53 (2005) 434–445.
[20] G.C. Wiggins, A. Potthast, C. Triantafyllou, C.J. Wiggins, L.L. Wald, Eight-channel phased array coil, detunable TEM volume coil for 7 T brain imaging, Magn. Reson. Med. 54 (2005) 235–240.
[21] J.R. Porter, S.M. Wright, A. Reykowski, A 16-element phased-array head coil, Magn. Reson. Med. 40 (1998) 272–279.
[22] Y.D. Zhu, C.J. Hardy, D.K. Sodickson, R.O. Giaquinto, C.L. Dumoulin, G. Kenwood, T. Niendorf, H. Lejay, C.A. McKenzie, M.A. Ohliger, N.M. Rofsky, Highly parallel volumetric imaging with a 32-element RF coil array, Magn. Reson. Med. 52 (2004) 869–877.
[23] M.P. McDougall, S.M. Wright, 64-channel array coil for single echo acquisition magnetic resonance imaging, Magn. Reson. Med. 54 (2005) 386–392.
[24] M. Schmitt, A. Potthast, D.E. Sosnovik, J.R. Polimeni, G.C. Wiggins, C. Triantafyllou, L.L. Wald, A 128-channel receive-only cardiac coil for highly accelerated cardiac MRI at 3 tesla, Magn. Reson. Med. 59 (2008) 1431–1439.
[25] G. Adriany, P.-F.v.d. Moortele, J. Ritter, S. Moeller, E.J. Auerbach, C. Akgün, C.J. Snyder, T. Vaughan, K. Ugurbil, A geometrically adjustable 16-channel transmit/receive transmission line array for improved RF efficiency and parallel imaging performance at 7 Tesla, Magn. Reson. Med. 59 (2008) 590–597.
[26] N. De Zanche, J.A. Massner, C. Leussler, K.P. Pruessmann, Modular design of receiver coil arrays, NMR Biomed. 21 (2008) 644–654.
[27] J.A. Nordmeyer-Massner, N. De Zanche, K.P. Pruessmann, Mechanically adjustable coil array for wrist MRI, Magn. Reson. Med. 61 (2009) 429–438.
[28] Fundamentals of RF and Microwave Noise Figure Measurements, Application Note 57-1 Agilent Technologies, 2004.
[29] C.N. Chen, D.I. Hoult, Biomedical Magnetic Resonance Technology, Adam Hilger, Bristol, UK, 1989.
[30] D.R. Chambers, A noise source for noise figure measurements, Hewlett-Packard J. April (1983) 26–27.
[31] W. Pastori, Programmable tuner commands impedances from 4 to 26.5 GHz, Microwaves & RF 28 (1989) 142–144.
[32] J.A. Massner, N. De Zanche, K.P. Pruessmann, A simple method to measure the noise figure of preamplifiers, Proc. ISMRM (2007) 328.
[33] D. Vondran, Noise figure measurement: corrections related to match and gain, Microwave J. 42 (1999) 22–38.
[34] Noise Figure Corrections, Application Note Anritsu, 2000.
[35] 10 Hints for Making Successful Noise Figure Measurements, Application Note 57-3 Agilent Technologies, 2000.
[36] J.B. Johnson, Thermal agitation of electricity in conductors, Phys. Rev. 32 (1928) 97–109.
[37] H. Nyquist, Thermal agitation of electric charge in conductors, Phys. Rev. 32 (1928) 110–113.
[38] R.Q. Lane, The determination of device noise parameters, Proc. IEEE 57 (1969) 1461–1462.
[39] G. Caruso, M. Sannino, Computer-aided determination of microwave two-port noise parameters, IEEE Trans. Microwave Theory Tech. 26 (1978) 639–642.
[40] M. Pavan, K.P. Pruessmann, A modular automatic matching network system, Proc. ISMRM (2010) 647.
[41] S. Wu, B.L. Beck, W.J. Turner, R. Bashirullah, T. Mareci, An automatic impedance matching system for multiple frequency coils, Proc. ISMRM (2010) 3920.
[42] C. Findeklee, Improving SNR by generalizing noise matching for array coils, Proc. ISMRM (2009) 508.